Journal of Sound and Vibration (1999) **227**(3), 523–544
Article No. jsvi.1999.2386, available online at http://www.idealibrary.com on IDEAL®

ANALYTICAL PREDICTIONS OF CHAOS IN A NON-LINEAR ROD

ALBERT C. J. LUO

*Department of Mechanical Engineering & Industrial Engineering, Southern Illinois University, Edwardsville, Edwardsville, IL*62026-1805, *U.S.A.*

AND

RAY P. S. HAN

*Department of Mechanical Engineering, University of Iowa, Iowa City, IA*52242-1527, *U.S.A.*

(*Received* 14 *October* 1998, *and in final form* 28 *April* 1999)

The resonant and chaotic conditions for non-dampened, non-linear, planar rods are developed through the Chirikov criterion, and the subharmonic bifurcation conditions for weakly dampened, non-linear, planar rods are also presented through the Melnikov method. The analytical conditions are based on a simply supported, geometrically non-linear, planar rod model with a specific single-mode response, but these conditions are applicable to geometrically non-linear planar rods with different supports. Chaos and transient motion from chaos to periodic motion in the non-linear rod are simulated through the approximate rod model, and they are illustrated through the Poincare mapping section.

1. INTRODUCTION

The accurate prediction of dynamic responses of an elastic rod experiencing large deformation is very significant in practice, and it relies on a more accurate beam theory describing such large deformation. The earlier beam theory developed by Kirchhoff was presented by Love [1]. In 1958, Erisksen and Truesdell [2] used the Cosserat approach [3] to develop an exact theory of stress and strain in rods and shells through the oriented bodies. In 1965, Green and Laws [4] extended this concept and developed a general theory of rods through two directors at each point in rods. Such theory is very difficult to apply in practice. In 1972, Reissner [5, 6] developed a one-dimensional finite-strain, static beam theory but how to treat the moment was not given. In 1973, Wempner [7] presented mechanics of curved rods but the strain is the Almansi–Hamel strain. The strain energy of non-linear rods was presented in reference [8]. In 1983, Maewal [9] gave strain–displacement relations in non-linear rods and shells. In 1987, Danielson and Hodges [10] discussed non-linear beam kinematics through the deposition of the rotation tensor, and a mixed variational formulation for dynamics of moving beams was

0022-460X/99/430523 + 22 $30.00/0

presented in reference [11]. Simo and Vu-Quoc [12] used the exact strain to develop a theory for geometrically nonlinear, planar rods, and several higher-order approximate theories were also given. Recently, this approach was used for development of the 3-D composite beam theory and numerical approaches were developed for prediction of dynamic responses in references [13–18]. The finite element modelling of geometrically non-linear beams in helicopters was also reported in references [19, 20]. The other derivation of equations of motion for geometrically non-linear rods can be found in references [21–25].

In 1972 the vibration of non-linear, planar rods based on an accurate beam theory was investigated through a perturbation approach [26]. The free, non-linear transverse vibration of beams was investigated in reference [27] when the beam properties varied along with length. Ho *et al.* [28, 29] discussed the non-linear vibration of rods through a single-mode model and a perturbation approach. The forced vibration of non-linear, torsional, inextensional beams was investigated in reference [30]. The planar, forced oscillations of shear indeformable beams was investigated through a specific, single-mode response and perturbation method [31] and the planar motion of an elastic rod under a compressive force was analyzed [32]. In 1981, Holmes and Marsden [33] used the Melnikov method to investigate the chaotic oscillation of a forced beam. Maewal [34] investigated chaotic motion in a harmonically excited elastic beam through the perturbation approach and Lyapunov exponent method. The dynamical potential for the non-linear vibration of cantilevered beams was discussed in reference [35], and the numerical simulations of chaotic motions in non-dampened non-linear rods were also presented. In 1984, Reichl and Zheng [36] used the Chirikov criterion presented in reference [37] to present an analytical condition for a stochastic layer in perturbed double-well systems. From the above literatures, the analytical prediction of chaos in non-linear rods still needs to be developed.

In this paper, an approximate model governing the large deformation of planar rods is presented. Based on this approximate theory, the conditions for chaos in non-dampened rods will be developed through the Chirikov overlap criterion, and the conditions for subharmonic bifurcation in dampened rods will be derived through the Melnikov method. Chaos in vicinity of resonant scparatrix for the non-dampened rod and transient motion to steady state periodic oscillation in the dampened rod are simulated numerically.

2. EQUATIONS OF MOTION

Consider the planar, non-linear vibration of a simply suported, initially straight, slender rod experiencing large deformation, and this rod is subjected to an axially compressive force P at the two ends, and a transverse, distributed, periodic force $q(x, t)$, as shows in Figure 1. The other planar rod models are found in references [25, 31, 32]. The geometrical relation and the exact axial strain [31] are

$$\sin\theta = \frac{w_{,x}}{\sqrt{(1+u_{,x})^2 + w_{,x}^2}}, \quad \cos\theta = \frac{1+u_{,x}}{\sqrt{(1+u_{,x})^2 + w_{,x}^2}} \tag{1}$$

$$\varepsilon_x = \varepsilon_0 + \sqrt{(1+u_{,x})^2 + w_{,x}^2} - 1, \tag{2}$$

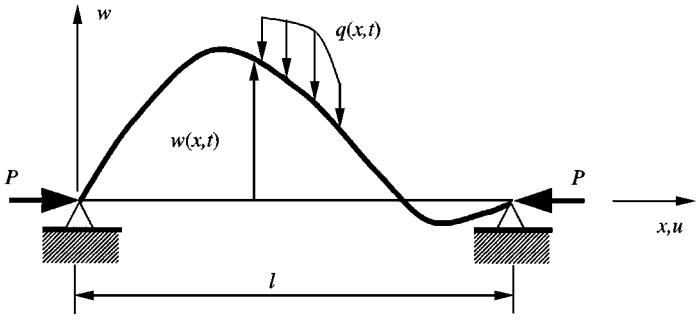

Figure 1. A non-linear, planar rod subjected to the compressive force P and transversely distributed loading $q(x, t)$.

where u and w are the longitudinal and transverse displacements of the middle surface, $\varepsilon_0 = P/EA$ is the initial strain and the $(\bullet)_{,x}$ denotes partial derivative with respect to x.

Similar to references [5, 26], the *equations* of motion for the large deformation of the planar rod are

$$\rho A\ddot{u} + \xi\dot{u} - (N\cos\theta - Q\sin\theta)_{,x} = 0, \quad \rho A\ddot{w} + \xi\dot{w} - (N\sin\theta - Q\cos\theta)_{,x} = q(t), \tag{3, 4}$$

$$-M_{,x} + Q[(1 + u_{,x})\cos\theta + w_{,x}\sin\theta] - N[w_{,x}\cos\theta - (1 + u_{,x})\sin\theta] \approx 0, \tag{5}$$

where N, Q and M are the normal force, shear force and bending moment; ρ and ξ are the density and damping coefficient of the rod, and the dot represents the derivative with respect to time. The slender rod is linear elastic and the moment and normal force [26] are

$$M = -\frac{EI[w_{,xx}(1 + u_{,x}) - u_{,xx}w_{,x}]}{[\sqrt{(1 + u_{,x})^2 + w_{,x}^2}]^3} \tag{6}$$

$$N(x, t) = -P + EA\varepsilon_x = -P + EA[\sqrt{(1 + u_{,x})^2 + w_{,x}^2} - 1], \tag{7}$$

where E, I and A are the Young's modulus, moment of inertia and cross-sectional area, respectively. Substitution of equation (1) into equation (5) gives

$$Q = \frac{M_{,x}}{\sqrt{(1 + u_{,x})^2 + w_{,x}^2}} \tag{8}$$

Substitution of equations (6)–(8) into equations (3) and (4) yields accurate equilibrium equations governing the large deformation of rod, i.e.,

$$\rho A\ddot{u} + \xi\dot{u} + \left(\left[\frac{(P + EA)}{\sqrt{(1 + u_{,x})^2 + w_{,x}^2}} - EA\right](1 + u_{,x}) - \frac{w_{,x}}{(1 + u_{,x})^2 + w_{,x}^2} \times \left\{\frac{EI[w_{,xx}(1 + u_{,x}) - u_{,xx}w_{,x}]}{[\sqrt{(1 + u_{,x})^2 + w_{,x}^2}]^3}\right\}_{,x}\right)_{,x} = 0, \tag{9}$$

$$\rho A\ddot{w} + \xi\dot{w} + \left(\left[\frac{(P+EA)}{\sqrt{(1+u_{,x})^2+w_{,x}^2}} - EA\right]w_{,x} - \frac{1+u_{,x}}{(1+u_{,x})^2+w_{,x}^2} \times \left\{\frac{EI[w_{,xx}(1+u_{,x}) - u_{,xx}w_{,x}]}{[\sqrt{(1+u_{,x})^2+w_{,x}^2}]^3}\right\}_{,x}\right)_{,x} = q(t). \tag{10}$$

The boundary conditions for the simply supported rod in Figure 1 is

$$u = w = u_{,xx} = w_{,xx} = 0 \quad \text{at } x = 0, l. \tag{11}$$

For development of an approximate theory for the rod, the following assumptions are adopted:

$$o(u) \ll o(w), \quad o(u_{,x}) \ll o(w_{,x}), \quad o(u_{,xx}) \ll o(w_{,xx}). \tag{12}$$

Use of the Taylor series expansion in equations (6) and (7), and retention of the lowest-order non-linear terms give

$$M \approx -EI[w_{,xx}(1 - 2u_{,x} - \tfrac{3}{2}w_{,x}^2) - u_{,xx}w_{,x}], \tag{13}$$

$$N(x,t) \approx -P + EA(u_{,x} + \tfrac{1}{2}w_{,x}^2). \tag{14}$$

From equation (12), the inertia and damping forces in equation (3) (or equation (9)) can be neglected, and integration of equation (3) gives

$$N\cos\theta - Q\sin\theta \approx e(t). \tag{15}$$

Because the rod is very slender, $Q\sin\theta \ll N\cos\theta$ can be proved through the non-dimensionalization analysis with equations (6), (8) and (12). When $Q\sin\theta$ is neglected in equation (15), equations (14) and (15) give

$$u_{,x} + \frac{1}{2}w_{,x}^2 \approx \frac{c(t)+P}{EA} = \frac{e(t)}{EA}. \tag{16}$$

The integration constant $c(t) = e(t) - P$ is determined through the axial force at the boundary in Figure 1. With equation (11), integration of equation (16) yields

$$u \approx -\frac{1}{2}\int_0^x w_{,x}^2\,\mathrm{d}x + \frac{x}{2l}\int_0^1 w_{,x}^2\,\mathrm{d}x. \tag{17}$$

Therefore, equation (17) becomes

$$u_{,x} \approx \frac{1}{2l}\int_0^1 w_{,x}^2\,\mathrm{d}x - \frac{1}{2}w_{,x}^2. \tag{18}$$

Note that the reduction of equation (3) can be completed as in references [26, 32]. Substitution of equation (18) into equation (10), use of the Taylor series expansion and retention of cubic terms gives an approximate equation of motion for the planar, geometrically non-linear rod, i.e.,

$$\rho A\ddot{w} + \xi\dot{w} + Pw_{,xx}\left(1 - \frac{1}{2l}\int_0^l w_{,x}^2\,\mathrm{d}x\right) - EAw_{,xx}\frac{1}{2l}\int_0^l w_{,x}^2\,\mathrm{d}x + EI\left[w_{,xxxx}\left(1 - \frac{3}{2l}\int_0^l w_{,x}^2\,\mathrm{d}x\right) + 2w_{,xxx}w_{,xx}w_{,x} + w_{,xx}^3\right] \approx q(x,t) \tag{19}$$

For the other boundary conditions of rods, the approximate equations of motion can be derived in a similar manner.

3. GALERKIN PROCEDURE

With equation (11), a solution to equation (19) is expressed as

$$w(x, t) = \sum_{m=1}^{\infty} F_m(t) \sin \frac{m\pi x}{l}. \tag{20}$$

For a specific m, application of the Galerkin method to equation (19) yields

$$\ddot{f} + \delta \dot{f} + \alpha_1 f + \alpha_2 f^3 \approx Q(t), \tag{21}$$

where

$$f(t) = \frac{m\pi F_m(t)}{l}, \qquad \alpha_1 = \frac{P_{mcr} - P}{a}, \qquad \alpha_2 = \frac{EA - 4P_{mcr} + P}{4a},$$

$$\delta = \frac{\xi}{m\pi a}, \quad a = \frac{\rho A l}{m\pi}, \quad P_{mcr} = \frac{(m\pi)^2 EI}{l^2}, \quad Q(t) = \frac{1}{2a} \int_0^l q(x, t) \sin \frac{m\pi x}{l} \, dx. \tag{22}$$

Consider $Q(t) = Q_0 \cos \Omega t$ as an example for illustration of chaotic motion. The coefficients α_1 and α_2 vary with the mode number m, the compressive force P and the material and geometrical properties. Therefore, there are four possible cases, i.e., Case I: $\alpha_1 > 0$ $\alpha_2 > 0$; Case II: $\alpha_1 > 0$ and $\alpha_2 < 0$; Case III: $\alpha_1 = 0$ and $\alpha_2 > 0$; Case IV: $\alpha_1 < 0$ and $\alpha_2 > 0$.

4. CHAOTIC CONDITIONS FOR A NON-DAMPENED ROD

4.1. CHAOTIC MOTION NEAR RESONANT SEPARATRIX

Consider chaotic motion in Case I ($\alpha_1 > 0$ and $\alpha_2 > 0$) of the non-linear rod. The first-order equations of equation (21) at $\delta = 0$ are

$$\dot{f} = y, \dot{y} = -\alpha_1 f - \alpha_2 f^3 + Q_0 \cos \Omega t, \tag{23}$$

and its Hamiltonian,

$$H = \tfrac{1}{2} y^2 + \tfrac{1}{2} \alpha_1 f^2 + \tfrac{1}{4} \alpha_2 f^4 - f Q_0 \cos \Omega t, \tag{24}$$

is expressed by $H = H_0 + H_1$, where

$$H_0 = \tfrac{1}{2} y^2 + \tfrac{1}{2} \alpha_1 f^2 + \tfrac{1}{4} \alpha_2 f^4 \quad \text{and} \quad H_1 = -f Q_0 \cos \Omega t, \tag{25}$$

For the conservative system in equation (23), its orbits in the phase plane for a given energy are qualitatively sketched in Figure 2. The solution of the conservative system for given $H_0 = E_0$ in equation (25) is [36–38]

$$f = h \operatorname{cn}\left[\frac{2K\theta}{\pi}, k\right] \text{ and } y = \pm \sqrt{\frac{\alpha_2}{2}} \frac{h^2}{k} \operatorname{sn}\left[\frac{2K\theta}{\pi}, k\right] \operatorname{dn}\left[\frac{2K\theta}{\pi}, k\right], \tag{26}$$

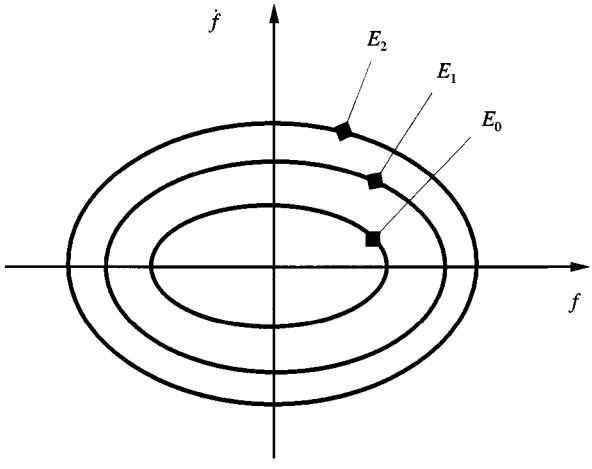

Figure 2. Conservative trajectories in the phase plane for the given energy of Case I.

where "cn", "sn", and "dn" are the Jacobian-elliptic functions, $K = K(k)$ is the complete elliptic integral of the first kind and k is its modulus. The amplitude h, the natural frequency ω and the phase θ of the solutions are

$$h = \sqrt{\frac{2k^2\alpha_1}{(1-2k^2)\alpha_2}}, \qquad \omega = \frac{1}{2}\sqrt{\frac{\alpha_2}{2}}\frac{h\pi}{kK} \quad \text{and} \quad \theta = \omega t. \tag{27}$$

The energy E_0 and the action variable J for a specific orbit are expressed by

$$E_0 = \frac{k^2(1-k^2)\alpha_1^2}{(1-2k^2)^2\alpha_2} \quad \text{and} \quad J = \frac{\sqrt{2\alpha_2}h^3}{3\pi k^3}[(1-k^2)K + (2k^2-1)E], \tag{28}$$

where $E = E(k)$ is the complete elliptic integral of the second kind. The period is computed by $T = 2\pi/\omega$. Substitution of equation (26) into equation (24) and the Fourier expansion of the time-dependent term give

$$H = H_0(J) - Q_0 \sum_{n=1}^{\infty} Q_{2n-1}\{\cos[(2\mathrm{n}-1)\omega - \Omega]t\cos\Omega t + \cos[(2n-1)\omega + \Omega]t\cos\Omega t\}, \tag{29}$$

where

$$Q_{2n-1} = \frac{\pi h}{2kK}\operatorname{sech}\left[\pi\left(n-\frac{1}{2}\right)\frac{K'}{K}\right], \quad K' = K(k') \text{ and } k' = \sqrt{1-k^2}. \tag{30}$$

Except for the $(2n-1)$th primary resonance, all other terms in H will average to zero over one period T in references [38, 39]. Hence, with equation (27), the resonant condition is

$$\omega = \frac{\Omega}{2n-1} = \frac{\pi}{2K(k)}\sqrt{\frac{\alpha_1}{1-2k^2}}. \tag{31}$$

From the foregoing the specific k for the $(2n-1)$th primary resonance and the given Ω can be determined, and this value is represented by k_{2s-1}. Further, the amplitude h and the action J corresponding to k_{2n-1} are represented by h_{2n-1} and J_{2n-1}. Chaotic motion in the neighborhood of the $(2n-1)$th resonant separatrix is of great interest. Only the contribution of the $(2n+1)$th resonance to the chaotic motion relative to the $(2n-1)$th resonant separatrix is considered, and the Hamiltonian H_0 in the neighborhood of the $(2n-1)$th resonant separatirx is expanded by a Taylor series. Therefore, equation (29) becomes

$$\begin{aligned} H \approx H_0(J_{2n-1}) + \left(\frac{\mathrm{d}H_0}{\mathrm{d}J}\right)_{J_{2n-1}} (J - J_{2n-1}) + \frac{1}{2}\left(\frac{\mathrm{d}^2 H_0}{\mathrm{d}J^2}\right)_{J_{2n-1}} (J - J_{2n-1})^2 + \cdots \\ - Q_0[Q_{2n-1}(J_{2n-1})\cos[(2n-1)\omega - \Omega]t \\ + Q_{2n+1}(J_{2n+1})\cos[(2n+1)\omega - \Omega]t\}. \end{aligned} \tag{32}$$

For introduction of a new canonical co-ordinate system $(\bar{p}, \bar{\phi})$ requiring $\bar{p} = 0$ when $J = J_{2n-1}$, a generating function is defined as

$$G(J, \bar{\phi}) = -(J - J_{2n-1})\left(\frac{\bar{\phi} + \Omega t}{2n-1}\right). \tag{33}$$

Therefore,

$$\bar{p} = -\frac{\partial G}{\partial \bar{\phi}} = \frac{J - J_{2n-1}}{2n-1} \quad \text{and} \quad \theta = \omega = -\frac{\partial G}{\partial J} = \frac{\bar{\phi} + \Omega t}{2n-1}. \tag{34}$$

Introduce a new Hamiltonian

$$\begin{aligned} \bar{H} = H + \frac{\partial G}{\partial t} \approx H_0(J_{2n-1}) - \frac{1}{2} B_0 (2n-1)^2 \bar{p}^2 \\ - Q_0 \left\{ Q_{2n-1}(J_{2n-1})\cos\bar{\phi} + Q_{2n+1}(J_{2n+1})\cos\left[\frac{2n+1}{2n-1}\bar{\phi} + \Omega_1 t\right]\right\}, \end{aligned} \tag{35}$$

where

$$\begin{aligned} B_0 = \left(\frac{d^2 H_0(J)}{dJ^2}\right)_{J_{2n-1}} = \frac{\pi^2}{4(h_{2n-1})^2 (K_{2n-1})^3}\left[K_{2n-1} - \frac{1 - 2(k_{2n-1})^2}{1 - (k_{2n-1})^2} E_{2n-1}\right] \\ \Omega_1 = \frac{2\Omega}{(2n-1)}, \frac{\partial G}{\partial t} = \left(\frac{\mathrm{d}H_0(J)}{\mathrm{d}J}\right)_{J_{2n-1}} (J - J_{2n-1}). \end{aligned} \tag{36}$$

The variables in equation (35),

$$\phi = \bar{\phi},\ p = \frac{(2n-1)^2(2n+1)B_0}{\Omega}\bar{p},\ H = \frac{(2n-1)^2(2n+1)^2 B_0}{\Omega^2}[\bar{H} - H_0(J_{2n-1})], \tag{37}$$

are re-scaled. Thus the re-scaled Hamiltonian is

$$H = \frac{1}{2}p^2 - U_0\cos\phi - V_0\cos\left(\frac{2n-1}{2n+1}\phi + \Omega_1 t\right), \tag{38}$$

where

$$U_0 = \frac{(2n-1)^2(2n+1)^2 B_0}{\Omega^2} Q_0 Q_{2n-1} \quad \text{and} \quad V_0 = \frac{(2n-1)^2(2n+1)^2 B_0}{\Omega^2} Q_0 Q_{2n+1}, \tag{39}$$

$$Q_{2n-1} = \frac{\sqrt{2}\Omega}{\sqrt{\alpha_2}(2n-1)\cosh\left[\pi(n-\frac{1}{2})K'_{2n-1}/K_{2n-1}\right]} \text{ and}$$

$$Q_{2n+1} = \frac{\sqrt{2}\Omega}{\sqrt{\alpha_2}(2n+1)\cosh\left[\pi(n+\frac{1}{2})K'_{2n+1}/K_{2n+1}\right]}. \tag{40}$$

The Chirikov resonance overlap condition in references [36–38] is written as

$$2\sqrt{U_0} + 2\sqrt{V_0} = 1. \tag{41}$$

From the foregoing, the chaotic condition for the onset of global stochasticity near the $(2n-1)$th resonant separatrix with the influence of the $(2n+1)$th resonance is

$$Q_0 = \frac{\Omega^2}{4(2n-1)^2(2n+1)^2 B_0}\left(\frac{1}{\sqrt{Q_{2n-1}} + \sqrt{Q_{2n+1}}}\right)^2. \tag{42}$$

For a given excitation frequency Ω, equation (31) gives the elliptic modulus k_{2n-1} (e.g., the $(2n-1)$th resonance). From equation (28) the constant E_0 for a specific resonance can be computed, and also the complete elliptic integral of the first and second kinds (K_{2n-1} and E_{2n-1}) and h_{2n-1} in equation (27) can be evaluated as well. From equations (30) and (36), the intermediate parameters Q_{2n+1}, Q_{2n-1}, B_0 can be determined. Finally, the excitation amplitude Q_0 is determined through equation (42). For a given Ω, the critical value of Q_0 is also constant for the specific resonance. For illustration of such a relationship, the resonant condition in equation (31) is illustrated in Figure 3(a) through excitation frequency Ω and conservative energy E_0 at $\alpha_1 = \alpha_2 = 1{\cdot}0$. The chaotic condition in equation (42) is shown in Figure 3(b) through excitation amplitude Q_0 and excitation frequency Ω.

The derivations for Cases II, III, IV(a) and (b) are similar to Case I; hence, the results are placed in Appendix A. Figure 4 shows the conservative orbits in the phase plane for the aforementioned four cases. The Case IV(c) will be discussed in the next section because it possesses a chaotic motion different from the above Cases.

The resonant conditions for Cases II–IV(b) are illustrated in the left plots of Figures 5–8 through the excitation frequency Ω and the conservative energy E_0 at $|\alpha_1| = |\alpha_2| = 1{\cdot}0$ The chaotic conditions for Case: II–IV(b) are shown in the right plots of Figures 5–8 through the excitation amplitude Q_0 and the excitation frequency Ω.

4.2. CHAOTIC MOTION NEAR HOMOCLINIC ORBIT

The chaotic motion in the neighborhood of the homoclinic orbit possessing $H_0 = 0$ is different from the Cases I–IV(b). The conservative orbits in the neighborhood of the homoclinic orbit are sketched in Figure 9, and the solution of

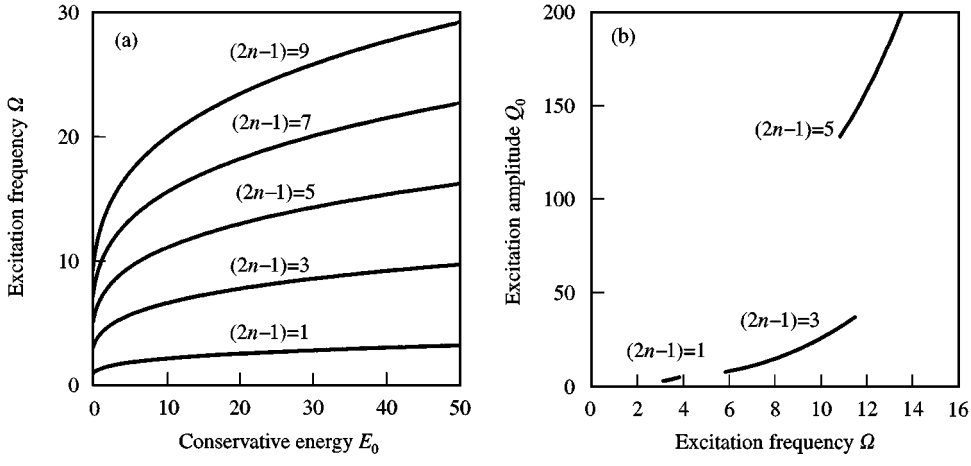

Figure 3. (a) Resonant condition and (b) chaotic condition for Case I of a non-dampened rod at $\alpha_1 = \alpha_2 = 1$.

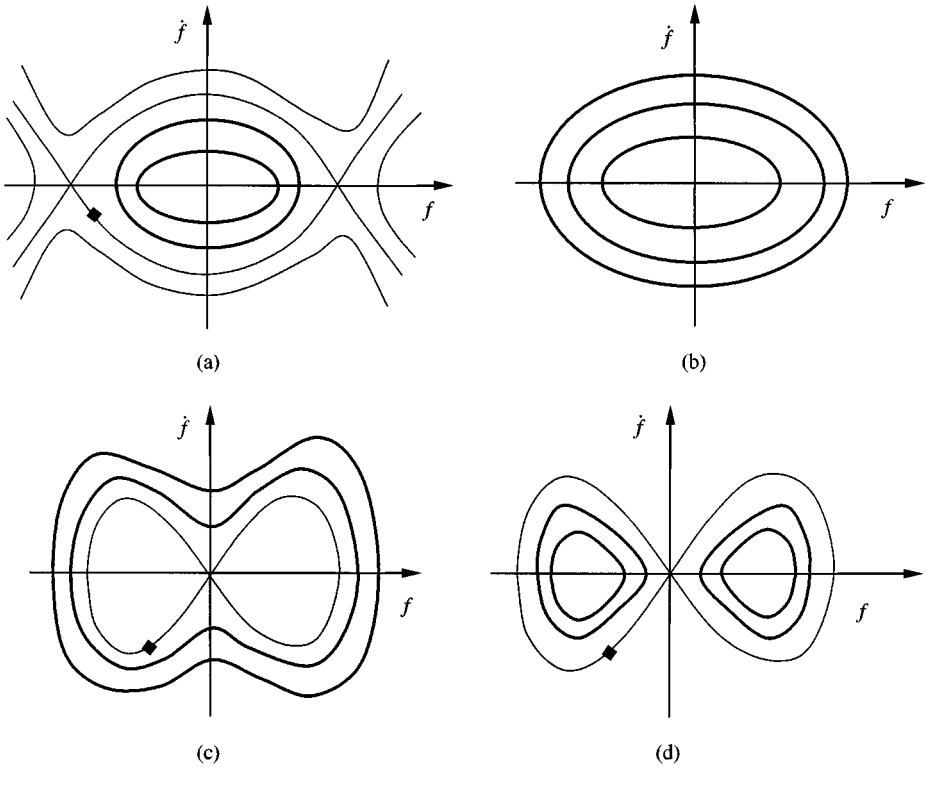

Figure 4. Conservative trajectories in phase plane: (a) Case II (heteroclinic orbit), (b) Case III, (c) Case IV(a) (homoclinic orbit), and (d) Case IV(b) (homoclinic orbit).

the homoclinic orbit is

$$f = \pm \sqrt{\frac{2|\alpha_1|}{\alpha_2}}\,\mathrm{sech}\,(\sqrt{\alpha_2}t) \quad \text{and} \quad y = \pm \sqrt{\frac{2}{\alpha_2}}\,|\alpha_1|\,\mathrm{sech}\,(\sqrt{\alpha_2}t)\tanh(\sqrt{\alpha_2}t). \tag{43}$$

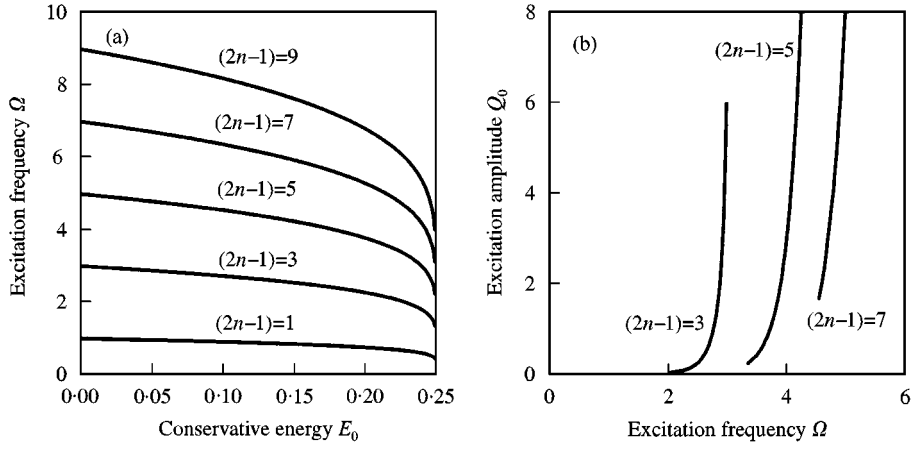

Figure 5. (a) Resonant condition and (b) chaotic condition for Case II of a non-dampened rod at $\alpha_1 = \alpha_2 = 1$.

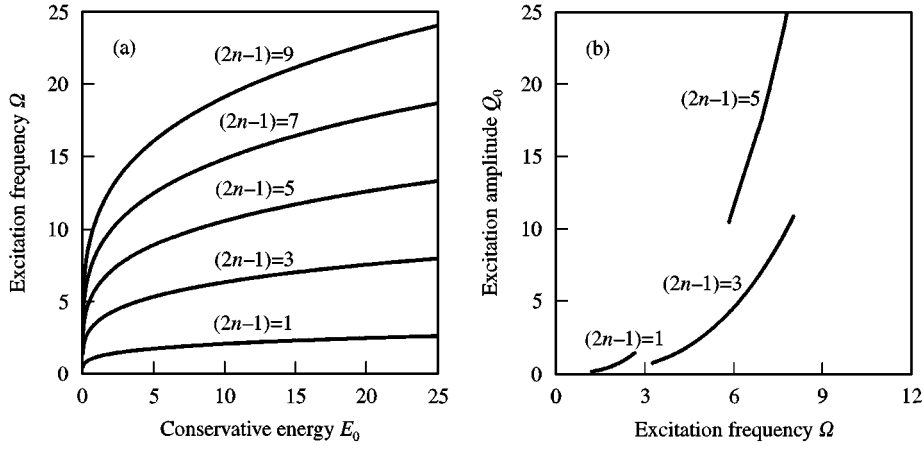

Figure 6. (a) Resonant condition and (b) chaotic condition for Case III of a non-dampened rod at $\alpha_1 = \alpha_2 = 1$.

Because $k \to 1$ as $E_0 \to 0$, the solutions of the conservative systems in Cases IV(a) and IV(b) approach to the homoclinic orbit. From Appendix A, the amplitude h, the conservative energy E_0 and the period T for Case IV(a) are approximated from

$$h \approx \sqrt{\frac{2|\alpha_1|}{\alpha_2}}, \quad E_0 \approx \frac{\alpha_1^2}{\alpha_2}(1-k^2) \text{ and } T \approx \frac{4\sqrt{2}kK}{\sqrt{\alpha_2}h}. \tag{44}$$

As in references [38, 40], the complete elliptic integral of the first kind as $k \to 1$ is approximated by

$$K \approx \frac{1}{2}\ln\left(\frac{16}{1-k^2}\right). \tag{45}$$

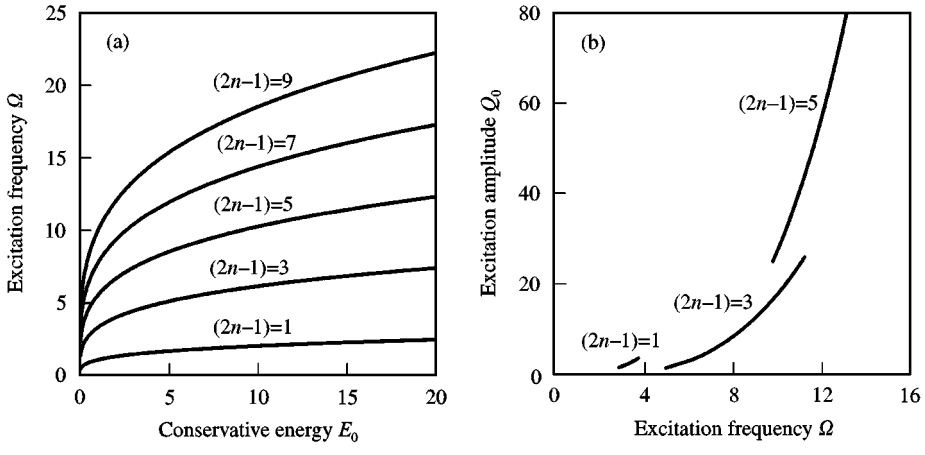

Figure 7. (a) Resonant condition and (b) chaotic condition for Case IV(a) of a non-dampened rod at $\alpha_1 = \alpha_2 = 1$.

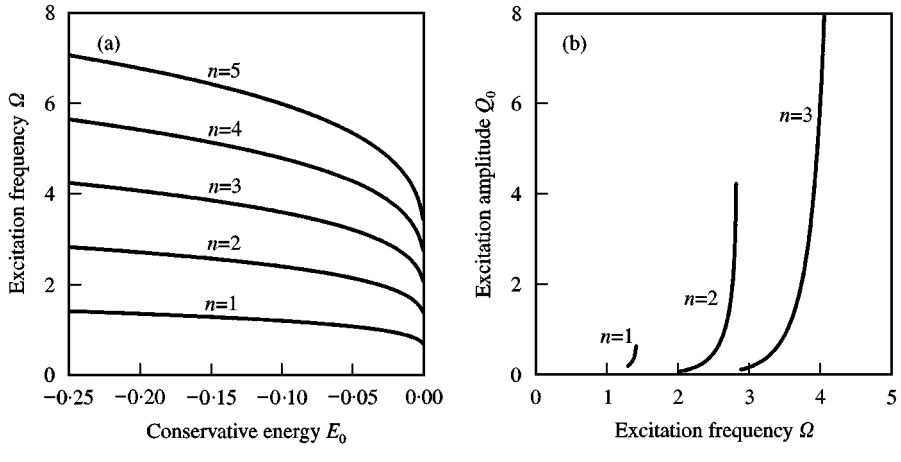

Figure 8. (a) Resonant condition and (b) chaotic condition for Case IV(b) of a non-dampened rod at $\alpha_1 = \alpha_2 = 1$.

Substitution of equation (45) into equation (44) results in

$$T \approx \frac{2}{\sqrt{|\alpha_1|}} \ln\left(\frac{16\alpha_1^2}{\alpha_2 E_0}\right). \tag{46}$$

The energy increment for one period T in reference [38] is

$$\Delta H = \lim_{T\to\infty} \int_{t_0}^{T+t_0} \left(\frac{\partial H_0}{\partial y}\frac{\partial H_1}{\partial f} - \frac{\partial H_0}{\partial f}\frac{\partial H_1}{\partial y}\right) \mathrm{d}t$$

$$\approx -Q_0 \pi\Omega \sqrt{\frac{2}{\alpha_2}}\, \mathrm{sech}\left(\frac{\pi\Omega}{2\sqrt{|\alpha_1|}}\right) \sin(\Omega t_0), \tag{47}$$

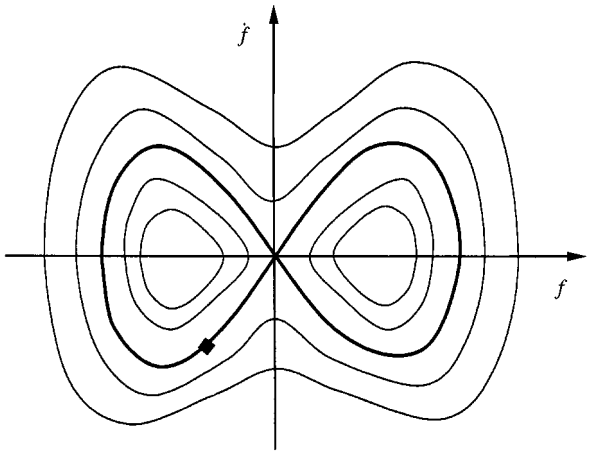

Figure 9. Homoclinic orbit and conservative trajectories in its neighborhood for Case IV(c).

where t_0 is the initial time and $\Delta H = E_{i+1} - E_i$. Let $E_0 = E_{i+1}$ in equation (46); the phase change of the trajectory for one period is

$$\Delta\phi = \phi_{i+1} - \phi_i = \Omega T \approx \frac{2\Omega}{\sqrt{|\alpha_1|}} \ln\left(\frac{16\alpha_1^2}{\alpha_2 E_{i+1}}\right). \tag{48}$$

The energy and phase relationships between the ith and $(i+1)$th iterations are

$$E_{i+1} \approx E_i - Q_0 \pi\Omega \sqrt{\frac{2}{\alpha_1}} \operatorname{sech}\left(\frac{\pi\Omega}{\sqrt{|\alpha_1|}}\right) \sin(\phi_i) \quad \text{and}$$

$$\phi_{i+1} = \phi_i + \frac{2\Omega}{\sqrt{|\alpha_1|}} \ln\left(\frac{16\alpha_1^2}{\alpha_2 E_{i+1}}\right), \tag{49}$$

which is a separatrix map. The period-1 fixed point of equation (49) requires

$$\frac{2\Omega}{\sqrt{|\alpha_1|}} \ln\left(\frac{16\alpha_1^2}{\alpha_2 E_1}\right) = 2\pi(2n-1) \quad \text{and} \quad \phi_1 = 0, \pi, \tag{50}$$

where E_1 is the energy at the period-1 fixed point. Let $E_i = E_1 + \Delta E_i$, linearization of the separatrix map in equation (49) at E_1 gives a standard map, i.e.,

$$w_{i+1} = w_i + D\sin(\phi_i) \text{ and } \phi_{i+1} = \phi_i + w_{i+1}, \tag{51}$$

where

$$w_i = -\frac{2\Omega}{\sqrt{|\alpha_1|}} \frac{\Delta E_i}{E_i} \quad \text{and} \quad D = \frac{2Q_0\pi\Omega}{E_1\sqrt{|\alpha_1|}} \sqrt{\frac{2}{\alpha_2}} \operatorname{sech}\left(\frac{\pi\Omega}{2\sqrt{|\alpha_1|}}\right). \tag{52}$$

The parameter D is termed the strength of the stochasticity. For the standard mapping, the transition to chaos occurs at $D^* \approx 0{\cdot}9716\ldots$ in reference [38]. The KAM torus will disappear and thus, the chaotic condition relative to the $(2n-1)$th

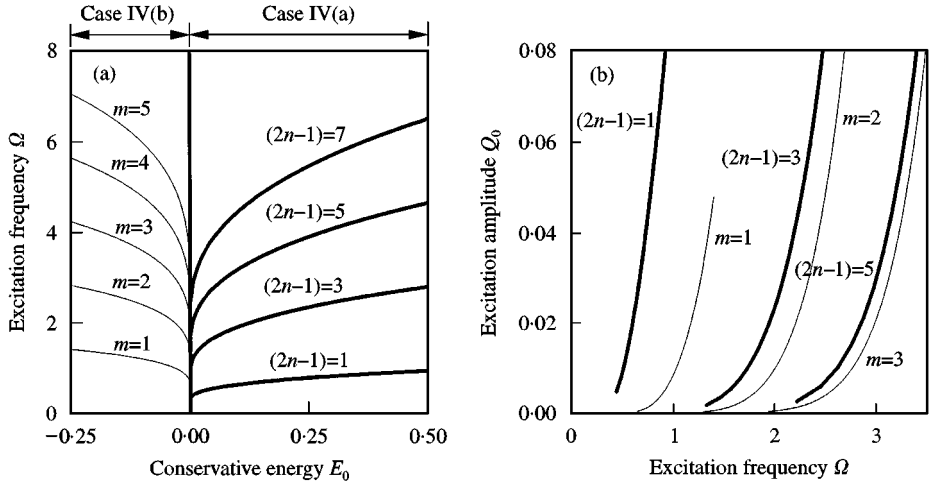

Figure 10. (a) Resonant condition and (b) chaotic condition for a non-dampened rod for Case IV(c) $|\alpha_1| = \alpha_2 = 1$ (——) Case IV(a); ——, Case IV(b)).

resonance outside the homoclinic orbit is

$$Q_0 \approx \frac{4D^*}{\pi}\left(\frac{|\alpha_1|}{\Omega}\right)\sqrt{\frac{|\alpha_1|}{2\alpha_2}}\,\mathrm{e}^{-[(2n-1)\pi\sqrt{|\alpha_1|/\Omega}]}\cosh\left(\frac{\pi\Omega}{2\sqrt{|\alpha_1|}}\right). \tag{53}$$

In a similar manner, the chaotic condition relative to the mth resonance inside the homoclinic orbit is

$$Q_0 \approx \frac{8D^*}{\pi}\left(\frac{|\alpha_1|}{\Omega}\right)\sqrt{\frac{|\alpha_1|}{2\alpha_2}}\,\mathrm{e}^{-(2m\pi\sqrt{|\alpha_1|/\Omega})}\cosh\left(\frac{\pi\Omega}{2\sqrt{|\alpha_1|}}\right). \tag{54}$$

As in Case I, the resonant conditions in neighborhood of the homoclinic orbit and the chaotic conditions in equation (53) and (54) are given in Figure 10 for $|\alpha_1| = |\alpha_2| = 1{\cdot}0$.

5. BIFURCATION CONDITION FOR A WEAKLY DAMPENED ROD

5.1. RESONANCE-BASED BIFURCATION

From equation (21), the equivalent system of first order equations is

$$\dot{f} = y,\ \dot{y} = -\alpha_1 f - \alpha_2 f^3 + \varepsilon(Q_0 \cos\Omega t - \delta\dot{f}). \tag{55}$$

As in reference [41], the Melnikov function for the foregoing at $\varepsilon = 1$ is

$$M^{(2n-1)}(t_0, Q_0, \delta, \Omega) = \int_{t_0}^{t_0+T} y[Q_0\cos(\Omega t - \delta y)]\,\mathrm{d}t = -\delta I_1 + Q_0 I_2 \sin\Omega t_0, \tag{56}$$

where $T = 2\pi/\omega$ is the period of the non-damped system and

$$I_1 = \frac{8}{3\alpha_2}\left(\sqrt{\frac{\alpha_1}{1-2k^2}}\right)^3 [(1-k^2)K + (2k^2-1)E],$$

$$I_2 = \frac{2\pi\sqrt{2}\Omega}{\sqrt{\alpha_2}} \operatorname{sech}\left[\left(n-\frac{1}{2}\right)\pi\frac{K'}{K}\right]. \tag{57}$$

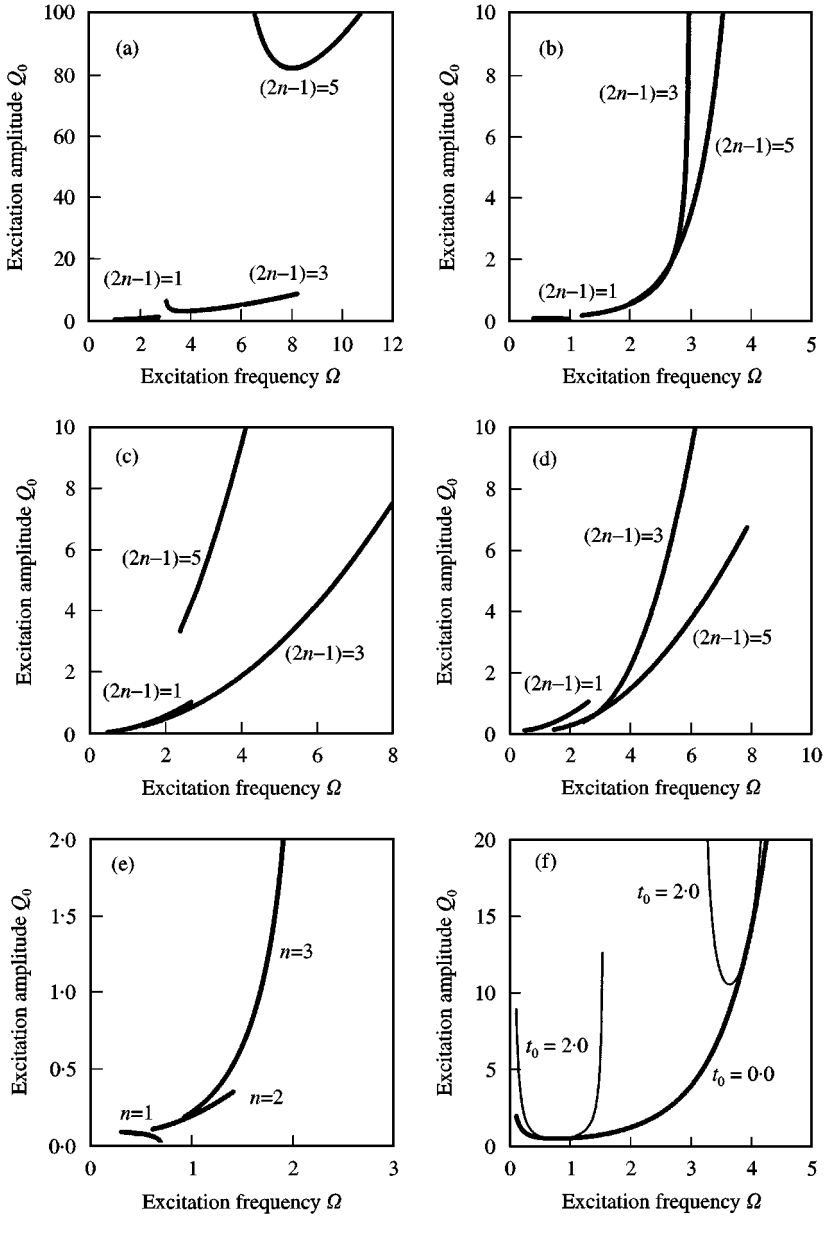

Figure 11. Subharmonic bifurcation conditions for the dampened rod ($\delta = 0{\cdot}5$) at $|\alpha_1| = |\alpha_2| = 1$: (a) Case I, (b) Case II, (c) Case III, (d) Case IV(a, b), (e) Case IV(b) and, (f) Case IV(c).

If $Q_0/\delta > I_1/I_2$, there is a $(2n-1)$th subharmonic periodic motion with $T = 2(2n-1)\pi/\Omega$. Thus, the subharmonic bifurcation condition in reference [41] is

$$Q_0 = \frac{I_1}{I_2}\,\delta. \tag{58}$$

Similarly, the conditions for the subharmonic bifurcations of Cases II–IV(b) is derived and the results are summarized in Appendix B.

5.2. HOMOCLINIC-ORBIT-BASED BIFURCATION

The Melnikov function in reference [41] is

$$M(t_0, Q_0, \delta, \Omega) = \int_{-\infty}^{\infty} y[Q_0 \cos\{\Omega(t+t_0) - \delta]\,\mathrm{d}t = -\delta I_1 + Q_0 I_2 \sin \Omega t_0, \tag{59}$$

where

$$I_1 = \frac{4(\sqrt{|\alpha_1|})^3}{3\alpha_2} \quad \text{and} \quad I_2 = \frac{2\pi\sqrt{2}\Omega}{\sqrt{\alpha_2}}\,\mathrm{sech}\left(\frac{\pi\Omega}{2\sqrt{|\alpha_1|}}\right). \tag{60}$$

The bifurcation condition for Case IV(c) can be expressed in equation (58). These bifurcation conditions for Cases I–IV(c) are also plotted in Figure 11 at $\delta = 0{\cdot}5$.

6. NUMERICAL SIMULATIONS

An adaptive Runge–Kuta integration scheme is used for illustration of chaotic motion in the non-linear rod through the Poincare mapping section. For observation of chaos in vicinity of a specific resonant separatrix relative to the given conserative energy E_0, the initial condition, excitation frequency and excitation amplitude should be computed analytically. The $(2n-1)$th resonance of Case I is used for explanation of the computation of input parameters for numerical simulations. For the given E_0, the $(2n-1)$th resonant separatrix in Case I can be determined through the conservative system of equation (38). As in reference [36–38], the hyperbolic points are at $\phi = 0, 2m_1\pi$ ($m_1 = 1, 2, \ldots$). The initial phase θ for specified m_1 can be computed by equation (34), and the initial condition (f_0, y_0) can be computed from equation (26), and (f_0, y_0) also satisfy $H_0 = E_0$ in equation (25). The elliptic modulus can be obtained from equation (28). The excitation frequency Ω can be computed through equation (31) and the critical excitation amplitude Q_0 for chaotic motion can be computed through equation (42). For the weakly damped rod, the excitation amplitudes Q_0 in the non-dampened rod are used, and the dampened coefficients are chosen for satisfaction of bifurcation condition. The computed input data is tabulated in Table 1. Because the chaotic motion of Cases III and IV(a) are similar to Case I, their numerical simulations will not be presented.

TABLE 1

Input data for numerical simulations ($\alpha_1 = \alpha_2 = 1$)

Figures	Types	Order of resonance	System input parameters			
			δ	(f_0, y_0)	Ω	Q_0
Non-dampened rod						
12(a)	Case I	3rd	/	(− 2·75723145, 0·00000000)	7.64562	13·092*
12(b)	Case II	3rd	/	(0·32752924, 0·45959614)	2·51708	0·305†
12(c)	Case I(b)	2nd	/	(1·27721125, 0·00000000) (R) (− 0·88066134, 0·41721017) (L)	2·57721	0·105‡
12(d)	Case IV(c)	3rd (inner) 5th (outer)	/	(0·00000000, 0·00000000)	3·00	0·06§
Dampened rod						
13(a)	Case I	3rd	0·001¶	(2·75723145, 0·00000000)	7·64562	13·092
13(b)	Case II	3rd	0·001¶	(− 0·32752924, 0·45959614)	2·51708	0·305
13(c)	Case IV(b)	2nd	0·001¶	(0·88066134, 0·41721017) (R) (− 1·27721125, 0·00000000) (L)	2·57721	0·105
13(d)	Case IV(c)	3rd (inner)	0·001¶	(0·00000000, 0·00000000)	3·00	0·06

*Predicted by Chirikov overlap crierion
†Less than $Q_0 = 0{\cdot}2598$ obtained through the Chirikov overlap criterion,
‡Less than $Q_0 = 0{\cdot}1257$ obtained by the analytical prediction,
§Greater than the critical values $Q_0 \approx 0{\cdot}0294$ for the 5th resonant separatrix outside of homoclinic orbit and $Q_0 \approx 0{\cdot}202$ for jthe 3rd resonant-separatrix inside of homoclinic orbit,
¶Less than critical damping value for periodic motion relative to the resonance.

The Poincare mapping sections of chaotic motions for Cases I, II, IV(b) and (c) of the non-dampened, non-linear rod are shown in Figure 12. From selection of the input data in Table 1, the chaotic motion in the neighborhood of the third resonant separatrix should be observed for Case I. In Figure 12(a) such chaotic motion relative to the third resonant separatrix is clearly shown. The chaotic motion in the neighborhood of the third resonant-separatrix of Case II is also simulated, as shown in Figure 12(b). For Case IV(b), the chaotic motions based on the second resonant sepatratix in the two potential wells are illustrated in Figure 12(c). The asymmetry of the chaotic motion in the two wells is observed even though the conservative trajectories in the two wells are symmetric. For Case IV(c), the chaotic motion in the neighborhood of the homoclinic orbit pertains to Cases IV(a) and (b). As analytically predicted, the 5th resonant separatrix outside the homoclinic orbit and the 3rd resonant separatrix in the two potential wells are observed in Figure 12(d), and the asymmetry of chaotic motions in the two wells is also observed.

The Poincare mappings of the transient motion from the chaotic motion to the steady state, periodic motion relative to the subharmonic resonance for Cases I, II, IV(b) and (c) of the weakly dampened rod are illustrated in Figure 13. For observation of periodic motion pertaining to subharmonic resonance, the damping for numerical simulations is less than the critical damping. For Case I, the transient

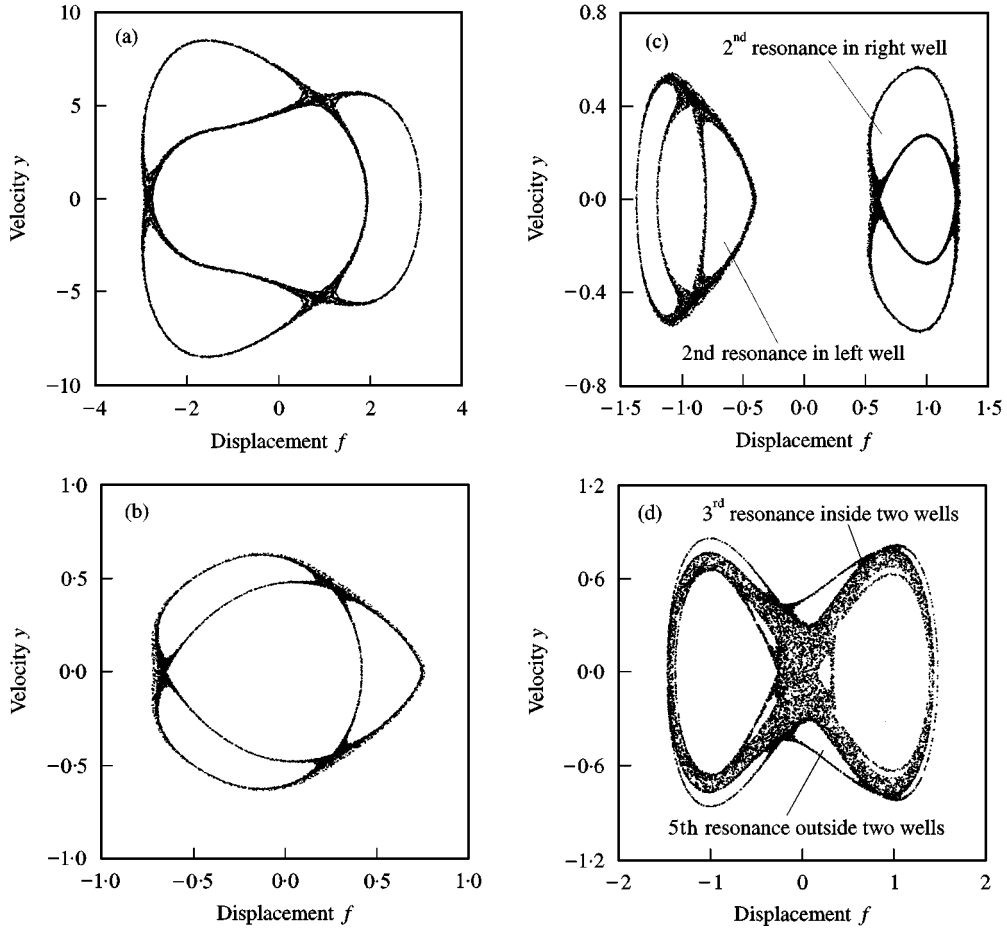

Figure 12. Poincare mapping sections of chaos in a non-dampened rod at $|\alpha_1| = |\alpha_2| = 1$: (a) Case I, (b) Case II, (c) Case IV(b), and, (d) Case IV(c).

motion from the chaotic motion to a steady state periodic motion relative to the 3rd resonance is illustrated in Figure 13(a). The period-3, subharmonic motion will be obtained as $t \to \infty$. If $\delta \geqslant 0{\cdot}195$, such periodic motion under the chosen excitation will not exist. Similarly, for Case II, a transient motion from the chaotic motion to a steady state, period-3 motion is shown in Figure 13(b). For Case IV(b), a transient motion from the chaotic motion to the steady-state, period-2 motions in the two potential wells are given in Figure 13(c). The locations of the period-2 motion in the two wells are very distinguishing. For Case IV(c), a transient motion from the chaotic motion to period-3 motion in the right potential wells is shown in Figure 13(d).

7. CONCLUSION

The resonant and chaotic conditions for non-dampened, non-linear, planar rods are derived, and the conditions for subharmonic bifurcation in weakly dampened,

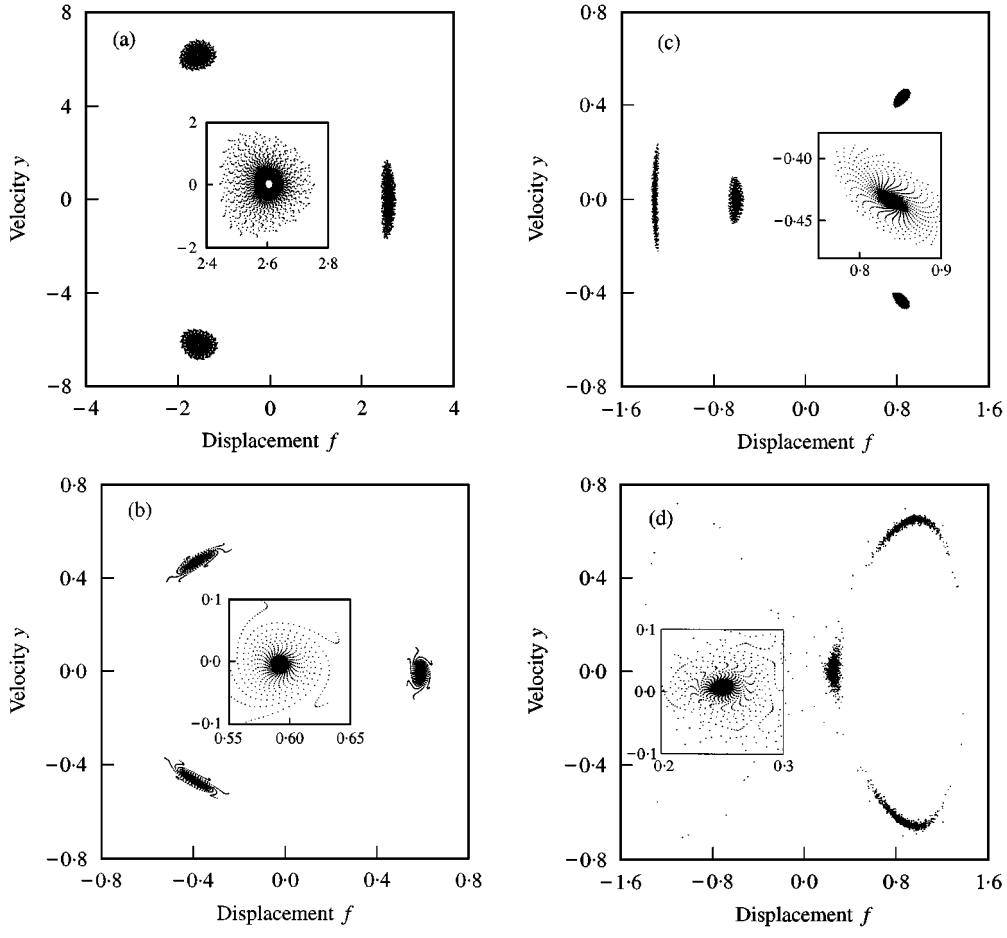

Figure 13. Poincare mapping sections of transient motion from chaotic to steady-state periodic motions in a dampened rod at $|\alpha_1| = |\alpha_2| = 1$: (a) Case I, (b) Case II, (c) Case IV(b), and, (d) Case IV(c).

non-linear, planar rods are also presented. The derivation of the analytical conditions is based on a simply supported, planar rod model, but these conditions are applicable to the planar rod models with different supports.

ACKNOWLEDGMENTS

The authors would like to thank the anonymous reviewers for their useful suggestions.

REFERENCES

1. A. E. H. Love 1944 *A Treatise on the Mathematical Theory of Elasticity*. New York: Dover Publications, fourth edition.
2. E. Cosserat and F. Cosserat 1909 *Theorie des Corps Deformables*, 953–1173. Paris: Appendix.

3. J. L. Erickensen and C. Truesdell 1958 *Archieves for Rational Mechanics and Analysis* **1**, 295–323. Exact theory of stress and strain in rods and shells.
4. A. E. Greene, F. R. S. and N. Laws 1966 *Royal Society of London Proceeding A* **293**, 145–155. A general theory of rods.
5. E. Reissner 1972 *Journal of Applied Mathematics and Physics* (*ZAMP*) **23**, 759–804. On one-dimensional finite-strain beam theory: the plane problem.
6. E. Reissner 1973 *Studies in Applied Mathematics* **LII**, 87–95. On one-dimensional large-displacement finite-strain beam theory: the plane problem.
7. A Waewal 1983 *Journal of Structural Mechanics* **10**, 393–401. A set of strain-displacement relations in nonlinear rod and shells.
8. V. L. Berdichevsky 1982 *PMM* **45**, 518–529. On the energy of an elastic rod.
9. G. Wempner 1973 *Mechanics of Solids with Application to Thin Body*. New York: McGraw-Hill.
10. D. A. Danielson and D. H. Hodge 1987 *ASME Journal of Applied Mechanics* **54**, 258–262. Nonlinear beam kinematics by decomposition of the rotation tensor.
11. D. H. Hodge 1990 *International Journal of Solids and Structures* **26**, 1253–1273. A mixed variational formulation based on exact intrinsic equations for dynamics of moving beams.
12. J. C. Simo and L. Vu-Quoc 1987 *Journal of Sound and Vibration* **119**, 487–508. The role of nonlinear theories in transient dynamics analysis of flexible structures.
13. J. C. Simo nd L. Vu-Quoc 1991 *International Journal of Solids and Structures* **27**, 371–393. A geometrically-exact rod model incorporating shear and torsion-warping deformation.
14. L. Vu-Quoc and I. K. Ebcioglu 1995 *ASME Journal of Applied Mechanics* **62**, 756–763. Dynamics formulation for geometrically-exact sandwich beams and 1-D plates.
15. L. Vu-Quoc and H. Deng 1995 *ASME Journal of Applied Mechanics* **62**, 479–488. Galerkin projection for geometrically-exact sandwich beams allows for play drop-off.
16. L. Vu-Quoc, H. Deng and I. K. Ebcioglu 1996 *Journal of Nonlinear Science* **6**, 239–270. Sandwich beams: a geometrically-exact formulation.
17. L. Vu-Quoc and I. K. Ebcioglu 1996 *Zeitschrift fur Angewande Mathematik und Mechanik* (*ZAMM*) **76**, 756–763. General multilayer geometrically-exact beams/1-D plate with piecewise linear section deformation.
18. L. Vu-Quoc and H. Deng 1997 *Computer Methods in Applied Mechanical and Engineering* **146**, 135–172. Dynamics of geometrically-exact sandwich beams: computational aspects.
19. M. Borri and P. Mantegazza 1985 *l'Aerotecnica Missili e Spazio* **64**, 143–159. Some contributions on structural dynamic modeling of helicopter rotor blades.
20. O. A. Bauchau and N. K. Kang 1993 *Journal of the American Helicopter Society* **38**, 3–14. A multibody formulation for helicopter structural dynamic analysis.
21. M. R. M. Crespo da Silva and C. C. Glynn 1978 *Journal of Structural Mechanics* **6**, 437–448. Nonlinear flexural–flexural–torsional dynamics of inextensional beams—I: equations of motion.
22. M. R. M. Crespo da Silva 1991 *Applied Mechanics Review* **44**, 51–59. Equations for nonlinear analysis of 3D motions of beams.
23. P. F. Pai and A. H. Nayfeh 1990 *Nonlinear Dynamics* **1**, 477–502. Three-dimensional nonlinear vibrations of composite beams—I: equation of motion.
24. P. F. Pai and A. H. Nayfeh 1992 *Nonlinear Dynamics* **3**, 273–303. A nonlinear composite beam theory.
25. P. F. Pai and A. H. Nayfeh 1994 *International Journal of Solids and Structures* **31**, 1309–1340. A fully nonlinear theory of curved and twisted composite rotor blades accounting for warping and three-dimensional stress effects.
26. G. R. Verma 1972 *Studies in Applied Mathematics* **LII**, 805–814. Nonlinear vibrations of beams and membranes.

27. A. H. Nayfeh 1973 *Journal of the Accoustical Society of America* **53**, 766–770. Nonlinear transverse vibration of beams with properties that vary along the length.
28. C. H. Ho, R. A. Scott and J. G. Eisley 1975 *International Journal of Nonlinear Mechanics* **10**, 113–127. Non-planar, nonlinear oscillations of beams—I: forced motions.
29. C. H. Ho, R. A. Scott and J. G. Eisley 1976 *International Journal of Sound and Vibration* **47**, 333–339. Non-planar, nonlinear oscillations of beams—II: free motions.
30. M. R. M. Crespo da Silva and C. C. Glynn 1978 *Journal of Structural Mechanics* **6**, 449–641. Nonlinear flexural–flexural–torsional dynamics of inextensional beams—II: forced motion.
31. A. Luongo, G. Rega and F. Vestroni 1986 *ASME Journal of Applied Mechanics* **53**, 619–624. On nonlinear dynamics of planar shear indeformable beams.
32. T. M. Atanackovic and L. J. Cveticanin 1996 *ASME Journal of Applied Mechanics* **63**, 392–398. Dynamics of plane motion of an elastic rod.
33. P. J. Holmes and J. Marsden 1981 *Archives for Rational Mechanics and Analysis* **76**, 135–166. A partial differential equation with infinitely many periodic orbits: chaotic oscillations of a forced beam.
34. A. Maewal 1986 *ASME Journal of Applied Mechanics* **53**, 625–631. Chaos in a harmonically excited elastic beam.
35. V. L. Berdichevsky, W. W. Kim and A. Ozbek 1995 *Journal of Sound and Vibration* **179**, 151–164. Dynamics potential for nonlinear vibrations of cantilevered beams.
36. L. E. Reichi and W. M. Zheng 1984 *Physical Review A* **30**, 1068–1077. Perturbed double-well system: the pendulum approximation and low-frequency effects.
37. B. V. Chirikov 1979 *Physics Reports* **52**, 263–379. A universal instability of many dimensional oscillator systems.
38. A. J. Lichtenberg and M. A. Lieberman 1992 *Regular and Chaotic Dynamics*. New York: Springer-Verlag.
39. A. C. J. Luo 1995 *Analytical modeling of bifurcations, chaos, and multifractals in nonlinear dynamics*. Ph.D. Dissertation, University of Manitoba, Winnipeg, Manitoba, Canada.
40. A. Cayley 1895 *Elliptic Functions*. London: Bells and Sons.
41. J. Guckenheimer and P. Holmes 1983 *Nonlinear Oscillations, Dynamical Systems and Bifurcation of Vector Fields*. Springer-Verlag: New York.

APPENDIX A: RESULTS FOR A NON-DAMPENED ROD

The results for Cases II, III, IV(a) and (b) are listed as follows.

Case II ($\alpha_1 > 0$ *and* $\alpha_2 < 0$):

$$E_0 = \frac{k^2\alpha_1^2}{(k+1)^2|\alpha_2|}, \quad h = \sqrt{\frac{2k^2\alpha_1}{(k+1)^2|\alpha_2|}}, \quad \omega = \frac{\sqrt{|\alpha_2|}h\pi}{2\sqrt{2}kK(k)}, \tag{A.1}$$

$$B_0 = \frac{\pi^2}{4h^2(k'_{2n-1})^2(K_{2n-1})^3}\left[K_{2n-1} - \frac{1+(k_{2n-1})^2}{1-(k_{2n-1})^2}E_{2n-1}\right], \tag{A.2}$$

$$Q_{2n-1} = \frac{\sqrt{2}\Omega}{\sqrt{|\alpha_2|}(2n-1)\sinh\left[\pi\left(n-\frac{1}{2}\right)\frac{K'_{2n-1}}{K_{2n-1}}\right]},$$

$$Q_{2n+1} = \frac{\sqrt{2}\Omega}{\sqrt{|\alpha_2|}(2n+1)\sinh\left[\pi\left(n+\frac{1}{2}\right)\frac{K'_{2n+1}}{K_{2n+1}}\right]}. \tag{A.3}$$

The chaotic condition for this case is identical to that of Case I.

Case III: $\alpha_1 = 0$ *and* $\alpha_2 > 0$:

$$k = \frac{1}{\sqrt{2}}, \quad h = \left(\frac{4E_0}{\alpha_2}\right)^{1/4}, \quad \omega = \frac{\sqrt{\alpha_2}h\pi}{2K(k)}, \quad B_0 = \frac{\pi^2}{2h^2(K_{2n-1})^2}, \tag{A.4}$$

$$Q_{2n-1} = \frac{\sqrt{2}\Omega}{\sqrt{|\alpha_2|}(2n-1)\cosh\left[\pi(n-\frac{1}{2})\right]},$$

$$Q_{2n+1} = \frac{\sqrt{2}\Omega}{\sqrt{|\alpha_2|}(2n+1)\cosh\left[\pi(n+\frac{1}{2})\right]}. \tag{A.5}$$

The chaotic condition for this case is expressed by equation (42).

Case IV(a): $\alpha_1 < 0$ *and* $\alpha_2 > 0$: Consider the conservative energy of Case IV: (a) $E_0 > 0$, (b) $E_0 < 0$, (c) $E_0 = 0$. Only the results for Cases IV(a) and (b) are given herein because the results for Case IV(c) have been presented in the paper.

For Case IV(a), we have

$$E_0 = \frac{(1-k^2)k^2\alpha_1^2}{(2k^2-1)^2\alpha_2}, \quad h = \sqrt{\frac{2k^2|\alpha_1|}{(2k^2-1)\alpha_2}}, \quad \omega = \frac{\sqrt{\alpha_2}h\pi}{2\sqrt{2}kK}, \tag{A.6}$$

$$B_0 = \frac{\pi^2}{4h^2(k_{2n-1})^3}\left[K_{2n-1} - \frac{1-2(k_{2n-1})^2}{1-(k_{2n-1})^2}E_{2n-1}\right], \tag{A.7}$$

$$Q_{2n-1} = \frac{\sqrt{2}\Omega}{\sqrt{\alpha_2}(2n-1)\cosh\left[\pi(n-\frac{1}{2})K'_{2n-1}/K_{2n-1}\right]},$$

$$Q_{2n+1} = \frac{\sqrt{2}\Omega}{\sqrt{\alpha_2}(2n+1)\cosh\left[\pi(n+\frac{1}{2})K'_{2n+1}/K_{2n+1}\right]}. \tag{A.8}$$

The chaotic condition for this case is expressed by equation (42).

For Case IV(b), we have

$$E_0 = \frac{(k^2-1)\alpha_1^2}{(2-k^2)^2\alpha_2}, \quad h = \sqrt{\frac{2|\alpha_1|}{(2-k^2)\alpha_2}}, \quad \omega = \frac{\sqrt{\alpha_2}h\pi}{2\sqrt{2}K}, \tag{A.9}$$

$$B_0 = \frac{\pi^2}{h^2(k_n)^4(k_n)^3}\left[K_n - \frac{2-(k_n)^2}{1-(k_n)^2}E_n\right], \tag{A.10}$$

$$Q_n = \frac{\sqrt{2}\Omega}{\sqrt{\alpha_2}\, n \cosh[n\pi K_n'/K_n]}, \quad Q_{n+1} = \frac{\sqrt{2}\Omega}{\sqrt{\alpha_2}(n+1)\cosh[\pi(n+1)K_n'/K_n]}, \tag{A.11}$$

$$Q_0 = \frac{\Omega^2}{4n^2(n+1)^2 B_0}\left(\frac{1}{\sqrt{Q_n}+\sqrt{Q_{n+1}}}\right)^2. \tag{A.12}$$

For this case, the chaotic condition presented in equation (A.13) is different from equation (41).

APPENDIX B: RESULTS FOR A WEAKLY DAMPENED ROD

The results for Cases II, III, IV(a) and (b) of a weakly dampened rod are listed herein.

Case II: $\alpha_1 > 0$ *and* $\alpha_2 < 0$:

$$I_1 = \frac{8}{3|\alpha_2|}\left(\sqrt{\frac{\alpha_1}{1}k^2}\right)^2 [(1+k^2)E - (1-k^2)K],$$

$$I_2 = \frac{2\pi\sqrt{2}\Omega}{\sqrt{|\alpha_2|}} \operatorname{csch}\left[\left(n-\frac{1}{2}\right)\pi\frac{K'}{K}\right]\sin(\Omega t_0). \tag{B.1}$$

Case III: $\alpha_1 = 0$ *and* $\alpha_2 > 0$:

$$I_1 = \frac{16[K(k)]^4\Omega^3}{3[(2n-1)\pi]^3\alpha_2}, \quad I_2 = \frac{2\pi\Omega}{\sqrt{\alpha_2}} \operatorname{sech}\left[\left(n-\frac{1}{2}\right)\pi\right]\sin(\Omega t_0). \tag{B.2}$$

Case IV(a): $\alpha_1 < 0$, $\alpha_2 > 0$ *and* $E_0 > 0$:

$$I_1 = \frac{8}{3\alpha_2}\left(\sqrt{\frac{|\alpha_1|}{2k^2-1}}\right)^3 [(2k^2-1)E + (1-k^2)K],$$

$$I_2 = \frac{2\pi\sqrt{2}\Omega}{\sqrt{\alpha_2}} \operatorname{sech}\left[\left(n-\frac{1}{2}\right)\pi\frac{K'}{K}\right]\sin(\Omega t_0). \tag{B.3}$$

Case IV(a): $\alpha_1 < 0$, $\alpha_2 > 0$ *and* $E_0 < 0$:

$$I_1 = \frac{4}{3\alpha_2}\left(\sqrt{\frac{|\alpha_1|}{2-k^2}}\right)^3 [(2-k^2)E - (1-k^2)K],$$

$$I_2 = \frac{\pi\sqrt{2}\Omega}{\sqrt{\alpha_2}} \operatorname{sech}\left[n\pi\frac{K'}{K}\right]\sin(\Omega t_0). \tag{B.4}$$

The bifurcation condition for all the cases is identical to equation (58).